Journal of Power Sources 219 (2012) 80–88

Contents lists available at SciVerse ScienceDirect

Journal of Power Sources

journal homepage: www.elsevier.com/locate/jpowsour

Preparation, surface characteristics, and electrochemical double-layer capacitance of KOH-activated carbon aerogels and their O- and N-doped derivatives

Zulamita Zapata-Benabithe [1], Francisco Carrasco-Marín, Carlos Moreno-Castilla*

Departamento de Química Inorgánica, Universidad de Granada, 18071 Granada, Spain

HIGHLIGHTS

- ► Carbon aerogels are KOH-activated at various weight ratios to increase their porosity.
- ► Oxygen and nitrogen functionalities are introduced by different surface treatments.
- ► The gravimetric capacitance is related to N_2 adsorption-measured microporosity.
- ► The gravimetric capacitance linearly decreases with increasing particle density.
- ► A volumetric capacitance as high as 123 F cm^{-3} is obtained with an O-doped carbon.

ARTICLE INFO

Article history:
Received 24 May 2012
Received in revised form
4 July 2012
Accepted 13 July 2012
Available online 20 July 2012

Keywords:
Activated carbon aerogels
Surface-treated activated carbon aerogels
Double-layer capacitance
Energy storage

ABSTRACT

Carbon aerogels are obtained by carbonizing organic aerogels prepared by polycondensation reaction of resorcinol or pyrocatechol with formaldehyde. They are KOH-activated at two KOH/carbon ratios to increase pore volume and surface area. Selected samples are also surface-treated to introduce oxygen and nitrogen functionalities. The objectives are to investigate the effect of porosity and surface functionalities on the electrochemical capacitance of the carbon and activated carbon aerogels. Samples are characterized by N_2 and CO_2 adsorption at −196 and 0 °C, respectively, immersion calorimetry, temperature-programmed desorption, and X-ray photoelectron spectroscopy in order to determine their surface area, porosity, and surface chemistry. Two series of samples are obtained: one micro-mesoporous and the other basically microporous. A surface area up to 1935 $m^2 g^{-1}$ was obtained after KOH activation. Electrochemical double-layer capacitance was studied by cyclovoltammetry and chronopotentiometry with a three-electrode cell, using Ag/AgCl as reference electrode. Gravimetric capacitance at 0.125 A g^{-1} is related to N_2 adsorption-measured micropore volume and mean size and to particle density. The highest gravimetric capacitance, 220 F g^{-1}, is obtained with two O- and N-doped samples. Volumetric capacitance of 123 F cm^{-3}, double the value generally needed for applications in small-volume systems, is obtained with a largely microporous oxygen-doped activated carbon aerogel.

1. Introduction

Electrochemical double layer (EDL) capacitors are a class of electrochemical energy storage devices with ideal characteristics for the rapid storage and release of energy [1]. This capability is mainly achieved by a non-faradaic mechanism through the separation of ions across a very small distance in the double-layer at the electrode/electrolyte interface, and it is dependent on the surface area of the electrode and the accessibility of the electrolyte to its porosity. Many carbon materials are good candidates for utilization as electrodes in EDL capacitors due to their high surface area and developed porosity [2,3] and there have been a number of reviews on their applications in these devices [4–7]. In addition, the EDL capacitance of carbon materials can be improved by faradaic reactions that introduce pseudocapacitance phenomena when surface functionalities such as oxygen and nitrogen complexes are present; these phenomena are attributable to changes in the acid/base character of the carbon surface and the presence of redox reactions [2,3,8–11].

Carbon gels are highly versatile porous carbon materials, whose surface area, porosity, and surface chemistry can be controlled by using the appropriate ingredients and preparation methods. They can be prepared with high purity or doped with other elements and are obtainable in a wide variety of forms, including pellets,

* Corresponding author. Tel.: +34 958 243323; fax: +34 958 248563.
E-mail address: cmoreno@ugr.es (C. Moreno-Castilla).
[1] Permanent address: Facultad de Ingeniería Química, Universidad Pontificia Bolivariana, 050031 Medellín, Colombia.

0378-7753/$ – see front matter © 2012 Elsevier B.V. All rights reserved.
http://dx.doi.org/10.1016/j.jpowsour.2012.07.036

microspheres, irregular-shaped powders, and films [12,13]. These characteristics make carbon gels highly suitable for applications as EDL capacitor electrodes [4–7,14–16].

The surface area and microporosity of carbon materials can be considerably enhanced by chemical activation with alkaline hydroxides [17–21], which impacts on their EDL capacitance. In the present study, carbon aerogels are prepared by carbonizing organic aerogels obtained from the polycondensation reaction of resorcinol or pyrocatechol with formaldehyde under basic or acid conditions, respectively. The resulting carbon aerogels are KOH-activated and surface-treated to introduce surface oxygen and nitrogen functionalities. The objective of this study is to determine the effects on EDL capacitance of the increase in surface area and porosity and the changes in surface chemistry.

2. Experimental

2.1. Sample preparation

Two organic aerogels, OR and OP, were prepared by the sol–gel polymerization reaction of resorcinol (R) or pyrocatechol (P) with formaldehyde (F) in water (W) using potassium carbonate or oxalic acid as catalyst (C), according to the recipes in Table 1. The R/F or P/F molar ratio was 0.5 and the R/W or P/W ratio was 0.132. The R/C and P/C molar ratios were 800 and 577, respectively. Mixtures were stirred to obtain a homogeneous solution that was cast into glass molds (45 cm length × 0.5 cm i.d.). Glass molds were sealed, and the mixtures were cured for 5 days at different temperatures up to 80 °C.

After the curing cycle, the gel rods were cut into 5 mm pellets and immersed in acetone to exchange water. Impregnated acetone pellets were dried with supercritical CO_2. Next, dried OR and OP aerogels were pyrolyzed in N_2 flow (300 cm^3 min^{-1}) at a heating rate of 1.5 °C min^{-1} up to 900 °C with a soaking time of 5 h. Carbon aerogels will be referred to henceforth as samples CR and CP, respectively.

Portions of CR and CP were chemically activated with KOH. For this purpose, both samples were ground and sieved between 0.5 and 1 mm and impregnated with a KOH aqueous solution to give KOH/carbon weight ratios of 2 and 4. The slurries were heated at 60 °C for 12 h and then at 100 °C to dryness. Samples were pyrolyzed in N_2 flow (300 cm^3 min^{-1}) at 300 °C for 3 h and then at 840 °C for 2 h at a heating rate of 10 °C min^{-1}. Chemically activated samples were washed with 0.1 M HCl and then with distilled water until absence of chloride ions in washing waters. Activated carbon aerogels are designated henceforth by appending the KOH/C weight ratio used, 2 or 4, to the names of the carbon aerogels (CR and CP).

Portions of CR4 and CP4 were treated with ammonium peroxydisulphate and melamine to introduce surface oxygen and nitrogen functionalities, respectively. The oxidation method with ammonium peroxydisulphate was similar to that described elsewhere [22]. Oxidized samples so obtained are designated henceforth as CR4O and CP4O. Melamine treatment was carried out by mixing 1 g of carbon and 2 g of melamine dissolved in 20 mL ethanol. The slurry was stirred, and the solvent slowly evaporated. The residue was heated in N_2 flow (300 cm^3 min^{-1}) at 750 °C for 1 h. This treatment largely followed a previously reported method [23]. Samples so obtained are designated henceforth as CR4N and CP4N.

Table 1
Organic aerogel recipes (formaldehyde, 0.224 mol; total water, 15.3 mL).

Sample	Resorcinol	Pyrocatechol	Catalyst	Initial pH
	mol	mol	mol	
OR	0.112	–	1.4×10^{-4} K_2CO_3	6.2
OP	–	0.112	1.94×10^{-4} $H_2C_2O_4$	1.7

2.2. Sample characterization

Surface area, pore texture, and surface chemistry were determined by N_2 and CO_2 adsorption at −196 and 0 °C, respectively, immersion calorimetry into benzene and water, temperature programmed desorption coupled with mass spectrometry (TPD) and X-ray photoelectron spectroscopy (XPS). Adsorption isotherms were measured with an Autosorb 1 from Quantachrome after outgassing samples overnight at 110 °C under high vacuum (10^{-6} mbar). N_2 adsorption isotherms were analyzed by BET equation, from which the surface area, S_{BET}, was obtained.

The Dubinin-Radushkevich (DR) equation was applied to N_2 and CO_2 adsorption isotherms at −196 and 0 °C, respectively, yielding the micropore volume, W_0, and the characteristic adsorption energy, E_0. The mean micropore width, L_0, was obtained by applying the Stoeckli [24] equation (1).

$$L_0(\text{nm}) = 10.8/(E_0 - 11.4\ \text{kJ mol}) \quad (1)$$

This equation is valid for E_0 values between 42 and 20 kJ mol^{-1}, which correspond to pore widths between 0.35 and 1.3 nm.

The volume of nitrogen adsorbed at a relative pressure of 0.95, $V_{0.95}$, was obtained from the N_2 adsorption isotherms, which, according to Gurvitch's rule, is equivalent to the addition of the micro- and meso-pore volumes. The mesopore volume, V_{meso}, was obtained from the difference between $V_{0.95}$ and $W_0(N_2)$.

Mesopore size distributions were obtained by applying the Barrett–Joyner–Halenda (BJH) method to the adsorption branch of N_2 adsorption–desorption isotherms of type IV in the IUPAC classification [25]. The mean size of mesopores, d_{BJH}, was calculated from these distributions. The particle density, ρ, was obtained by mercury picnometry at atmospheric pressure.

Immersion enthalpies into benzene, $-\Delta H_{benz}$, and water, $-\Delta H_{water}$, were determined with a C80-D Setaram calorimeter. Samples were previously outgassed overnight under a dynamic vacuum of 10^{-6} mbar at 120 °C. Measurements were carried out at 30 °C and at least twice for each sample. Both immersion enthalpies were used to determine the hydrophobicity (HF) of the samples according to equation (2)

$$\text{Hydrophobicity} = 1 - (\Delta H_{water}/\Delta H_{benz}) \quad (2)$$

TPD was performed by heating samples up to 1000 °C at 10 °C min^{-1} and analyzing the CO and CO_2 evolved by means of a model Prisma mass spectrometer from Pfeiffer. The total oxygen content, O_{TPD}, was calculated from the amount of CO and CO_2 evolved. The total N content, N_{CHN}, was determined by elemental analysis.

XPS was performed by using an Escalab 200R system (VG Scientific Co.) equipped with MgK_α X-ray source ($h\gamma = 1253.6$ eV) and hemispherical electron analyzer. Survey and multi-region spectra were recorded at C_{1s}, O_{1s}, and N_{1s} photoelectron peaks. Each spectral region of photoelectron interest was scanned several times to obtain good signal-to-noise ratios. The C_{1s} peak at 284.6 eV was used as internal standard. Given that the depth recorded with this technique is around 2–3 nm below the external surface, it gives the surface content of oxygen, O_{XPS}, or nitrogen N_{XPS}.

2.3. Electrochemical measurements

Electrochemical measurements were carried out in a Biologic multichannel potentiostat at room temperature using 1 M H_2SO_4 as

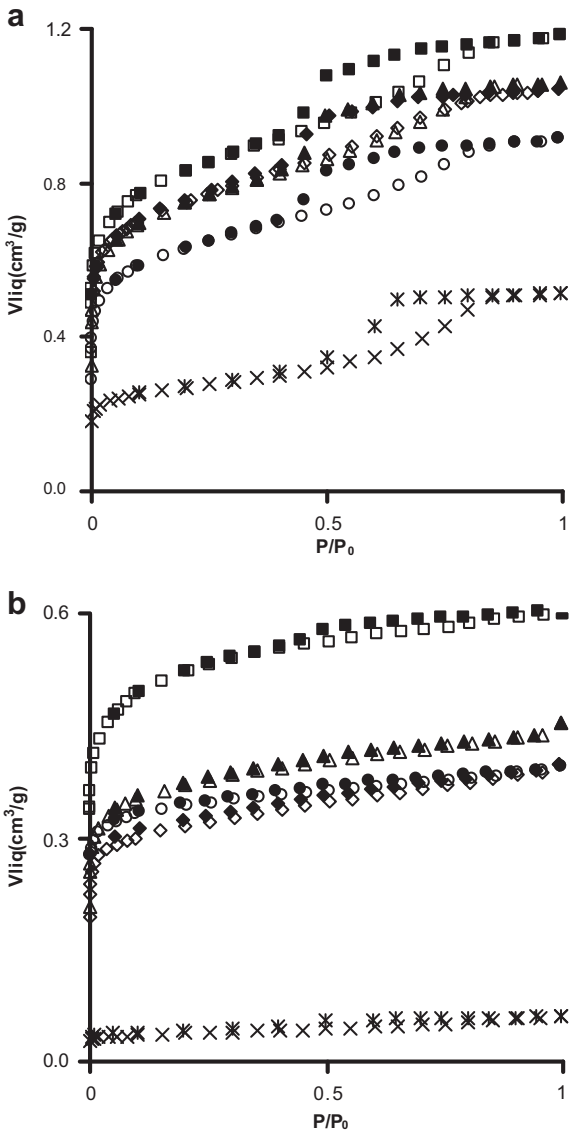

Fig. 1. N_2 adsorption–desorption isotherms on samples: a) CR (×, *), CR2 (◇, ◆), CR4 (□, ■), CR4O (○, ●) and CR4N (△, ▲); b) CP (×, *), CP2 (◇, ◆), CP4 (□, ■), CP4O (○, ●) and CP4N (△, ▲).

electrolyte, a typical three-electrode cell with Ag/AgCl as reference electrode, and Pt wire as counter electrode. The working electrode was a graphite paper pasted with a homogeneous mixture of the finely ground carbon aerogel or activated carbon aerogel, acetylene black, and binder (polytetrafluoroethylene, PTFE) at a mass ratio of 80:10:10.

Cyclic voltammograms (CVs) were obtained at different scan rates, and the gravimetric capacitance, C_{CV} (F g^{-1}), was calculated from these curves by equation (3)

$$C_{CV} = \frac{\sum |I| \Delta t}{2m\Delta V} \quad (3)$$

where $\Sigma|I|\Delta t$ is the area of the current (A) against time (s) curve, m the mass of active material in the electrode (g), and ΔV the potential window (V). Chronopotentiograms were performed at current loading between 0.125 and 1 A g^{-1} in a potential interval of 0–0.75 V. The gravimetric capacitance, C_{CP} (F g^{-1}), was obtained from these measurements by equation (4)

$$C_{CP} = \frac{I_d \Delta t}{m\Delta V} \quad (4)$$

where I_d is the discharge current (A), Δt the discharge time (s), and ΔV the potential interval (V).

3. Results and discussion

Carbonization of the organic aerogel pellets OR and OP gives rise to a similar weight loss of around 58%, with a reduction in diameter (shrinkage) of 29.8% (sample OR) and 41.3% (sample OP).

3.1. Porosity and surface area

Fig. 1a and b depicts the N_2 adsorption–desorption isotherms on the different activated carbon aerogels and their respective O- and N-derivatives. The isotherms on the CR series belong to type IV and show a hysteresis loop of type H2 according to the IUPAC classification [25]. The initial part of these isotherms, at low relative pressures, corresponds to micropore filling. Subsequently, the adsorption rises steeply with increases in relative pressure due to capillary condensation in mesopores. At high relative pressures, the amount adsorbed reaches a limiting value equal to the sum of micro- and meso-pore volumes. Figure 1S in Supplementary data depicts the mesopore size distribution obtained by applying the BJH method to these isotherms.

By contrast, the isotherms on the CP series belong to type I, typical of microporous solids. However, these samples also contain some mesopores, because the N_2 uptake slightly increases at a higher relative pressure after micropore filling. The adsorption and desorption branches of the isotherms practically coincide in these samples. We highlight that CP exhibits a type I N_2 adsorption isotherm, whereas another sample (POX-900) [26], prepared with the same ingredients (see Table 1) but a higher volume of water (26.7 mL) and pH (2.1), gives rise to type IV N_2 adsorption isotherms. This indicates that the amount of water used in the

Table 2
Porosity and surface area of the carbon aerogels, activated carbon aerogels, and their O- and N-doped derivatives.

		CR	CR2	CR4	CR4O	CR4N	CP	CP2	CP4	CP4O	CP4N
$W_0(N_2)$	$cm^3\ g^{-1}$	0.26	0.74	0.77	0.58	0.69	0.04	0.30	0.49	0.34	0.35
$W_0(CO_2)$	$cm^3\ g^{-1}$	0.27	0.59	0.53	0.41	0.49	0.13	0.30	0.34	0.34	0.31
$L_0(N_2)$	nm	1.15	1.30	1.20	1.13	1.19	0.88	0.73	0.96	0.84	0.84
$L_0(CO_2)$	nm	0.65	0.82	0.86	0.70	0.86	0.85	0.63	0.66	0.63	0.66
$V_{0.95}$	$cm^3\ g^{-1}$	0.51	1.04	1.18	0.91	1.06	0.05	0.40	0.61	0.40	0.45
V_{meso}	$cm^3\ g^{-1}$	0.25	0.30	0.41	0.33	0.37	0.01	0.10	0.12	0.06	0.10
L_{BJH}	nm	5.6	3.4	3.8	3.8	3.8	nd[a]	nd	nd	nd	nd
ρ	$g\ cm^{-3}$	0.61	0.46	0.40	0.51	0.36	0.88	0.83	0.64	0.75	0.64
S_{BET}	$m^2\ g^{-1}$	640	1796	1935	1470	1750	90	772	1255	855	898

[a] nd: not determined.

recipe and hence the solution pH have a marked impact on the mesoporosity of the final carbon aerogel and therefore on the shape of the N_2 adsorption isotherm.

KOH-activation considerably increases the N_2 uptake of carbon aerogels CR and CP at all relative pressures. Table 2 compiles the porosity and surface area obtained from the adsorption isotherms. The micropore volume obtained from CO_2 adsorption at 0 °C yields the volume of narrow micropores or ultramicropores (below about 0.7–0.8 nm width), whereas the total micropore volume is obtained from N_2 adsorption at −196 °C if there are no very narrow micropores or pore constrictions at their entrance [27,28].

Both micropore volumes are similar in sample CR, indicating a homogeneous microporosity. KOH-activation of CR increases the micropore volume and results in $W_0(N_2) > W_0(CO_2)$. The microporosity values of CR2 and CR4 are similar; therefore, the increase in KOH/carbon weight ratio from 2 to 4 has no effect on this type of porosity. However, KOH-activation and the rise in KOH/carbon ratio increase the V_{meso} of sample CR. This effect has been documented for activated carbons and carbon gels [17–21]. Activation reduces the L_{BJH} and the density, in this case due to the increased porosity.

Conversely, $W_0(N_2) < W_0(CO_2)$ for sample CP, indicating the presence of micropores that have very narrow or constricted entrances, preventing the access of N_2 molecules at −196 °C. KOH-activation of CP increases both micropore volumes, and the increase in KOH/carbon weight ratio results in $W_0(N_2) \geq W_0(CO_2)$. The V_{meso} value of CP increases with the activation, but the mesopore volume is considerably lower in these samples than in the CR series. Activation also decreases the particle density due to the increase in porosity. These results demonstrate that the CR activated carbon aerogel samples are micro-mesoporous materials, whereas the CP samples are basically microporous.

Fixation of surface oxygen functionalities on CR4 to obtain CR4O reduces the $W_0(N_2)$, $W_0(CO_2)$ and V_{meso} but not the L_{BJH}. Oxidation of CP4 to obtain CP4O reduces the $W_0(N_2)$ and V_{meso}. The reduction in porosity is attributable to its blocking by surface oxygen functionalities and/or to the destruction of micro- and meso-pore walls by the oxidizing treatment. The decrease in pore volumes brings about, as expected, an increase in particle density.

The introduction of surface nitrogen functionalities in sample CR4 to produce sample CR4N also reduces pore volumes, although the decrease is not as drastic as that produced by the oxidizing treatment. However, the changes in porosity in sample CP4N are similar to those in CP4O.

S_{BET} increases with higher KOH/carbon weight ratio during the chemical activation of the carbon aerogels, reaching a surface area as high as 1935 $m^2\ g^{-1}$ for sample CR4. The introduction of surface oxygen or nitrogen functionalities reduces the S_{BET} value.

3.2. Surface chemistry

Table 3 compiles the amounts of CO and CO_2 evolved up to 1000 °C, the O_{TPD} and O_{XPS} contents, the immersion enthalpies, $-\Delta H_{benz}$ and $-\Delta H_{water}$, and the hydrophobicity of the samples. In the case of the non-oxidized samples, $O_{TPD} < O_{XPS}$, which is typical of many carbon materials and is produced by oxygen chemisorption on the external carbon surface after exposure to the atmosphere. However, $O_{TPD} > O_{XPS}$ in the oxidized samples CR4O and CP4O, indicating that the oxidizing treatment mainly fixes the surface oxygen complexes within the carbon pores.

The amount of CO evolved up to 1000 °C is always higher than the amount of CO_2 evolved. The CO_2- and CO-desorption profiles of the samples with increased oxygen content, CR4O and CP4O, are depicted in Fig. 2. The CO_2-desorption profile of both samples show a well-defined peak corresponding to the maximum desorption rate at around 210–220 °C, due to the decomposition of carboxyl acid groups [22,29]. A small CO desorption peak appears in the same region and likely derives from the decomposition of carbonyl

Table 3
Amounts of CO and CO_2 evolved up to 1000 °C, oxygen contents, immersion enthalpy into benzene and water, and hydrophobicity (HF) of the carbon aerogels, activated carbon aerogels, and their O- and N-doped derivatives.

Sample	CO	CO_2	O_{TPD}	O_{XPS}	$-\Delta H_{benz}$	$-\Delta H_{water}$	HF
	mmol g^{-1}	mmol g^{-1}	wt%	wt%	J g^{-1}	J g^{-1}	
CR	0.15	0.04	0.37	5.7	86.8	21.5	0.75
CR2	1.01	0.24	2.38	nd	nd	nd	nd
CR4	0.85	0.13	1.78	5.9	215.0	66.6	0.69
CR4O	6.55	3.36	21.23	17.2	183.6	206.4	−0.12
CR4N	0.19	0.04	0.04	6.1	198.2	59.6	0.70
CP	0.31	0.10	0.82	7.6	nd	nd	nd
CP2	0.81	0.47	2.80	nd	nd	nd	nd
CP4	0.86	0.22	2.08	7.9	149.8	51.1	0.66
CP4O	4.39	2.24	14.19	12.1	134.2	114.5	0.15
CP4N	0.13	0.05	0.37	6.9	127.6	38.3	0.70

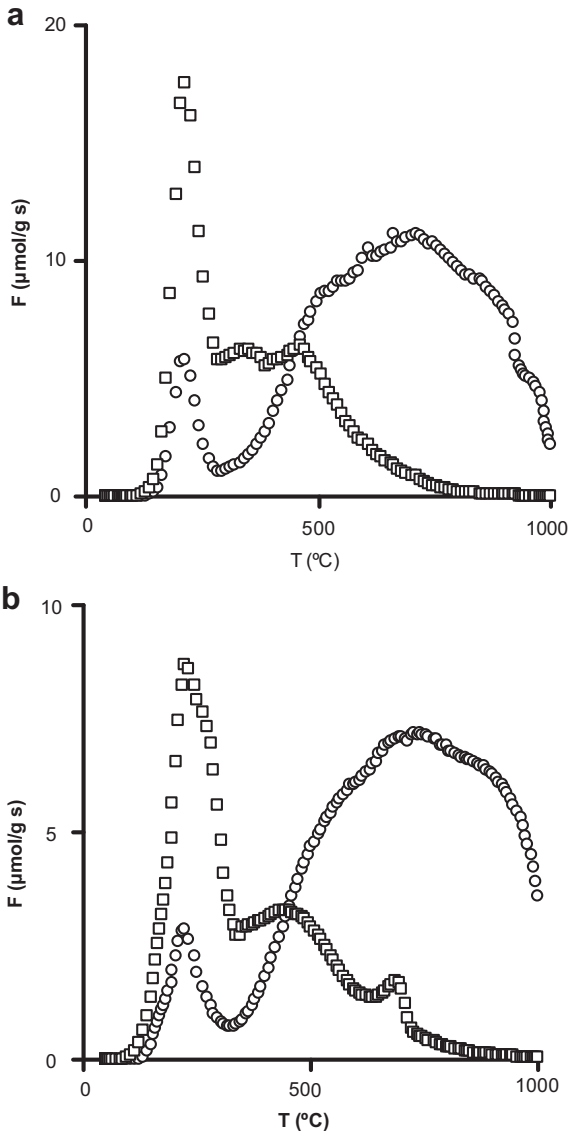

Fig. 2. CO_2 (□) and CO (○) desorption profiles from TPD of samples: a) CR4O and b) CP4O.

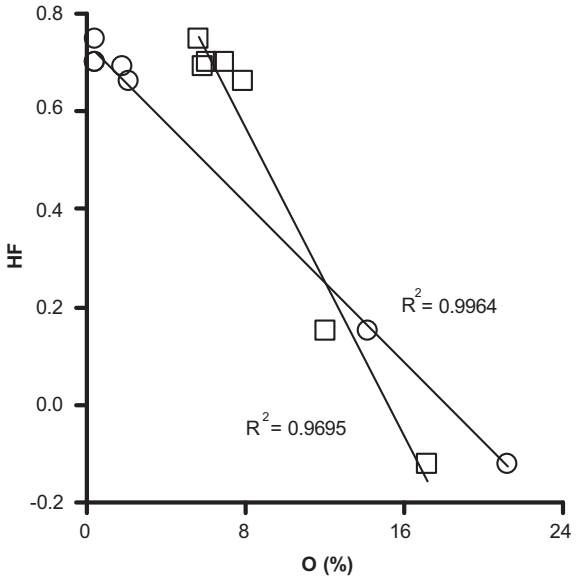

Fig. 3. Relationship between the hydrophobicity (HF) and the surface (○) and total (□) oxygen content of the samples.

Table 4
Weight percentages of total (N_{CHN}) and surface (N_{XPS}) nitrogen contents and N functionalities.

Sample	N_{CHN}	N_{XPS}	N-6	N-5	N-Q	N-X
CR4N	1.7	1.4	40	37	18	5
CP4N	1.5	1.4	35	34	23	8

groups into α-substituted ketones and aldehydes [22,30]. After the maximum in the CO_2-desorption profile, there is a tail up to around 1000 °C, with several shoulders and plateaus indicating the presence of chemically different functionalities such as lactones and anhydrides, or the same oxygen functionality at energetically different sites [31].

Interestingly, sample CP40 shows a CO_2 desorption peak at a high temperature (675 °C) that is close to the maximum (720 °C) of the CO-desorption profile. This is because there is a secondary reaction at this temperature, e.g., the Boudouard reaction, in which the evolved CO collides with other surface oxygen complexes, producing CO_2 [32,33]. This reaction likely takes place in CP4O and not in CR4O because the former is a microporous sample with negligible mesoporosity and a smaller $L_0(N_2)$. Hence, CP40 offers more favorable conditions for the collision of CO molecules with surface oxygen complexes on micropore walls in comparison to CR4O.

The CO-desorption profiles of both samples are very similar. After the first CO desorption peak reported above, a wide desorption peak is seen with a maximum centered at 720 °C. This peak corresponds to the desorption of functionalities such as anhydrides, phenol, carbonyl, hydroquinones, and quinone-like structures.

When electrochemical measurements are carried out in aqueous acid solutions, quinone and hydroquinone groups originate pseudocapacitance through redox reactions. In addition, the CO_2-evolving groups have an acid character and introduce electron-acceptor properties on the carbon surface that also contribute to the overall capacitance through pseudocapacitance interactions [10].

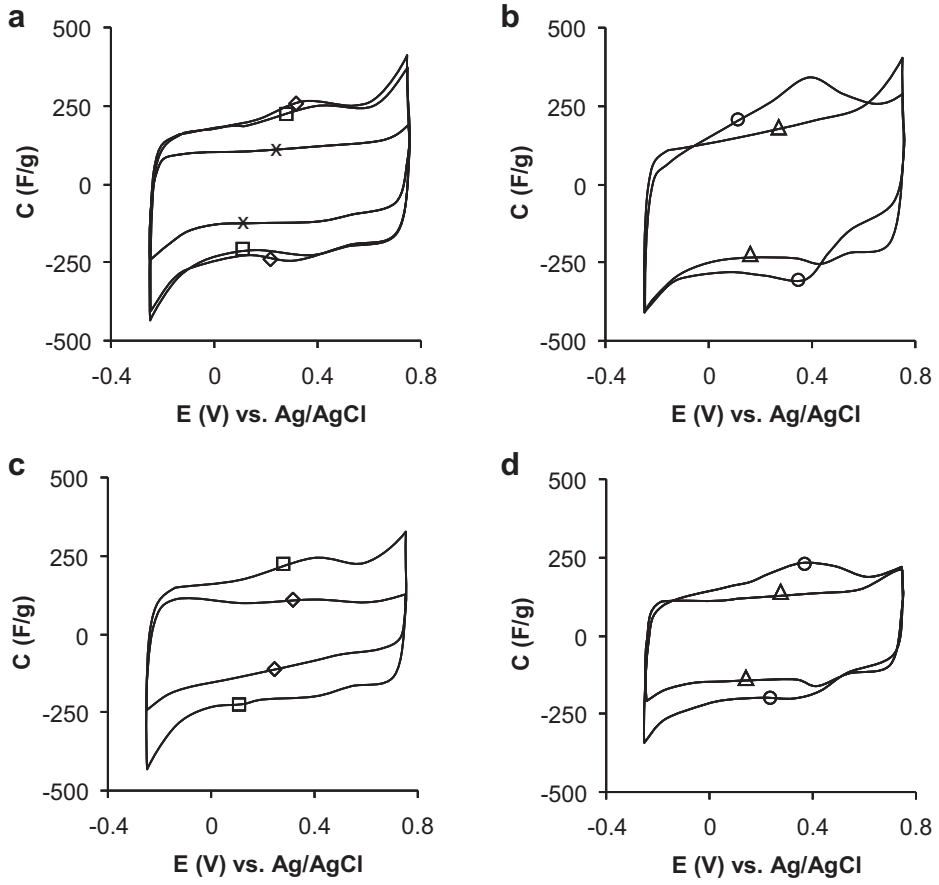

Fig. 4. Cyclic voltammograms in 1 M H_2SO_4 at 0.5 mV s^{-1} of samples: a) CR (×), CR2 (◇), CR4 (□); b) CR4O (○), CR4N (△); c) CP2 (◇) CP4 (□) and d) CP4O (○), CP4N (△).

Fig. 3 shows that the hydrophobicity diminishes linearly with an increase in the oxygen content, either O_{TPD} or O_{XPS}, attributable to the increased number of hydrophilic polar sites with oxygen content. This improves the wettability of the carbon surface by the electrolyte, facilitating the EDL formation. However, this advantage can be offset by the binding of oxygen polar groups (mainly carboxyl groups) with water molecules, hindering and retarding the migration of the electrolyte into the pores, thereby increasing the ohmic resistance.

The O_{1s} XP spectra of CR4O and CP4O are depicted in Supplementary data, Figure 2S. The deconvoluted spectra show two peaks at 531.6 and 533.1 eV, corresponding to double C═O bonds and single C–OH bonds [34], respectively. In both samples, the relative surface concentrations of these functionalities are 35 and 65%, respectively. Therefore, functionalities with single C–OH bonds such as carboxyl, hydroquinone, and phenol groups predominate in these oxidized samples.

The N_{1s} XP spectra of CR4N and CP4N are given in Supplementary data, Figure 3S. The spectra show peaks at: 398.7 eV (N-6), 400.6 eV (N-5), and 401.0 eV (N-Q) and a fourth peak between 402 and 405 eV (N–X) The N-6 and N-5 peaks correspond to pyridinic and pyrrolic or pyridonic nitrogen, respectively. The N–Q peak corresponds to quaternary nitrogen. The fourth peak, N–X, is due to certain forms of nitrogen oxide and nitrate structures [35–37].

N-6 and N-5 functionalities at the graphene layer edges enhance the carbon basicity [38] through a strong π delocalization in graphene layers, due to the electron-rich nature of these nitrogen sites. Therefore, protons from the electrolyte can be attracted to the electrode surface, giving rise to pseudocapacitive interactions [39]. N–Q functionalities are localized within the graphene layers and produce a major increase in the HOMO energy of the graphene sheet [40]. Because of this increased HOMO energy, graphene sheets with N–Q functionalities are more positively charged when used as anode material in supercapacitors, attracting more negatively-charged ions and increasing the capacitance.

Table 4 lists the relative surface concentrations of these functionalities and the total and surface N contents, N_{CHN} and N_{XPS}, respectively. These two values are similar, indicating a homogeneous N distribution between the bulk and the surface of the samples. N-6 and N-5 predominate in both N-doped activated carbon aerogels. The original activated carbon aerogels, CR4 and CP4, contain no nitrogen.

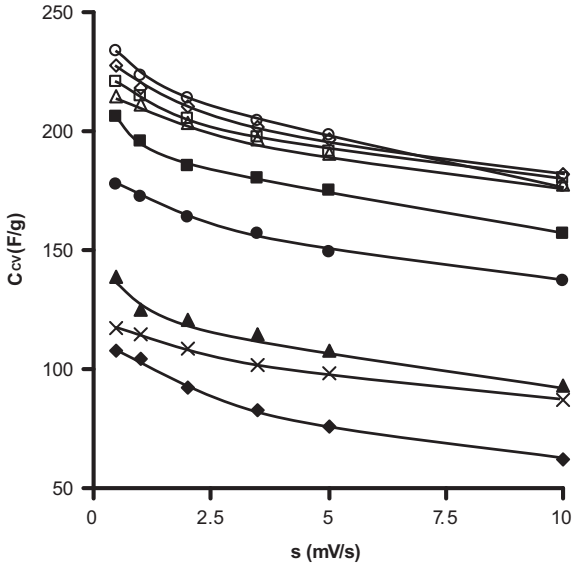

Fig. 5. Variation of the gravimetric capacitance (C_{CV}) with scan rate. Samples CR (×), CR2 (◇), CR4 (□), CR4O (○), CR4N (△), CP2 (◆), CP4 (■), CP4O (●), and CP4N (▲).

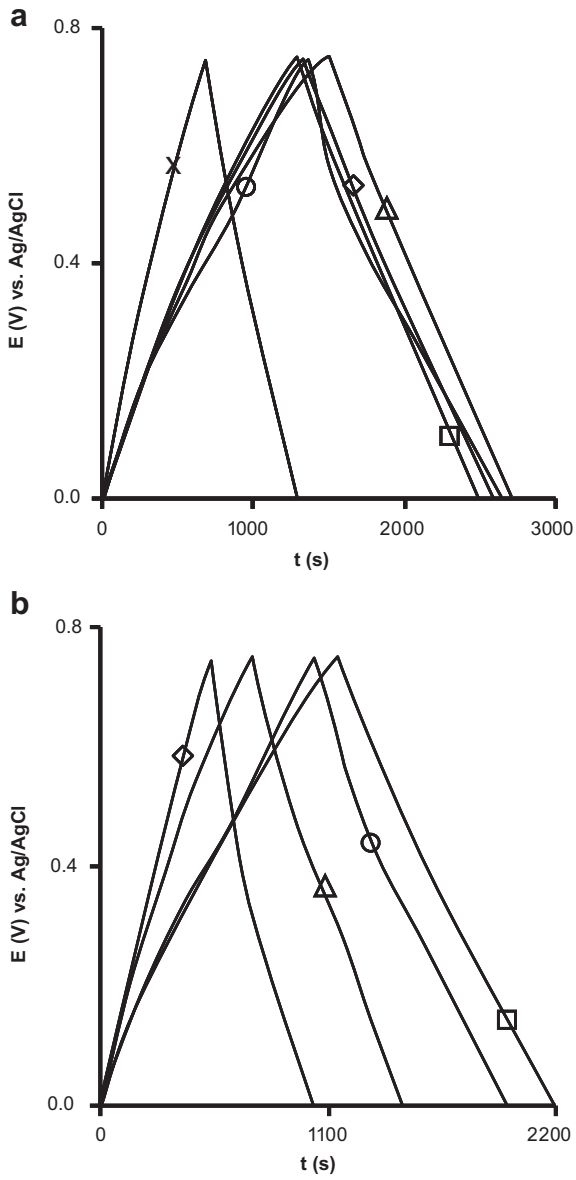

Fig. 6. Chronopotentiograms in 1 M H_2SO_4 at 0.125 A g^{-1} of samples: a) CR (×), CR2 (◇), CR4 (□), CR4O (○) and CR4N (△); b) CP2 (◇), CP4 (□), CP4O (○) and CP4N (△).

Table 5
Gravimetric (C_{CP}) and volumetric (VC_{CP}) capacitances at 0.125 A g^{-1}, and retention capacitance at 1 A g^{-1}.

Sample	C_{CP} F g^{-1}	VC_{CP} F cm^{-3}	Retention %
CR	107	65	78
CR2	217	100	82
CR4	208	83	82
CR4O	221	113	82
CR4N	224	81	83
CP2	92	76	71
CP4	183	117	73
CP4O	164	123	72
CP4N	122	78	73

3.3. Electrochemical double-layer capacitance

Fig. 4a–d depicts typical CVs at 0.5 mV s^{-1}. Samples CR, CR2, CR4 and CP4 exhibit CV profiles with a quasi-rectangular shape. In addition, CVs of the activated carbon aerogels CR2, CR4 and CP4 show small peaks between 0.3 and 0.4 V attributable to pseudofaradaic quinone/hydroquinone redox reactions [2]. These redox peaks are more pronounced in the oxidized samples, CR4O and CP4O, because of their higher oxygen content *versus* CR4 and CP4, respectively. The N-doped activated carbon aerogels CR4N and CP4N also show quasi-rectangular CV profiles, with a small peak around 0.4 V in the positive sweep that may be related to a pseudofaradaic contribution of surface nitrogen groups.

The CV shape of the activated carbon aerogel CP2 is non-rectangular and asymmetric with a decrease in current at high potential, indicating a deviation from the ideal double-layer capacitor. This CV narrowing at high potentials is a consequence of diffusional limitations of the hydrated bisulfate ions into the micropores, which produces an ion-sieving effect [41,42]. Thus, the size of these ions [43] is around 0.53 nm, and the $L_0(N_2)$ value of sample CP2 is the narrowest (0.73 nm) among all studied samples.

As shown in Fig. 5, the gravimetric capacitance C_{CV} decreases when the scan rate increases because the formation of the EDL within the micropores is slower and less complete in comparison to the rate of variation in potential. Fig. 6a and b depicts typical chronopotentiograms at a constant current load of 0.125 A g^{-1}. Application of equation (4) to these curves provides the gravimetric capacitance, C_{CP}, values in Table 5. Samples CR4O and CR4N show the highest gravimetric capacitance among all samples studied. The slightly higher capacitance than that of their parent sample (CR4) may be due to pseudofaradic effects introduced by the high oxygen content of CR4O and N content of CR4N. However, the pseudofaradaic contributions to the total capacitance of CP4O and CP4N with regard to CP4 are not detectable.

Fig. 7a shows that C_{CP} increases with higher total micropore volume within the range studied and reaches its maximum value when $W_0(N_2)$ is between 0.6 and 0.75 cm^3 g^{-1}. In addition, C_{CP} linearly increases with $L_0(N_2)$ within the range studied (Fig. 7b). These results show the importance of the volume and mean size of the total microporosity in the EDL formation. Finally, C_{CP} linearly decreases when the particle density increases within the range studied (Fig. 7c), due to the decrease in porosity.

However, besides the gravimetric capacitance, a high volumetric capacitance is important for all practical applications. This involves the use of carbon electrode materials with a high density, which is often incompatible with a developed porosity. Table 5 shows the volumetric capacitance, VC_{CP}, at 0.125 A g^{-1}. Sample CP4O has the highest VC_{CP} value among studied samples, 123 F cm^{-3}, although its C_{CP} value is not as high as that of samples CR4O and CR4N, due to the higher ρ value (smaller micro and mesopore volumes) of CP4O. The elevated VC_{CP} value found is two-fold higher than that generally demanded [4,44] for practical applications, 60 F cm^{-3}. This excellent result makes sample CP4O especially suitable for use in small-volume devices, e.g. in microelectronics systems.

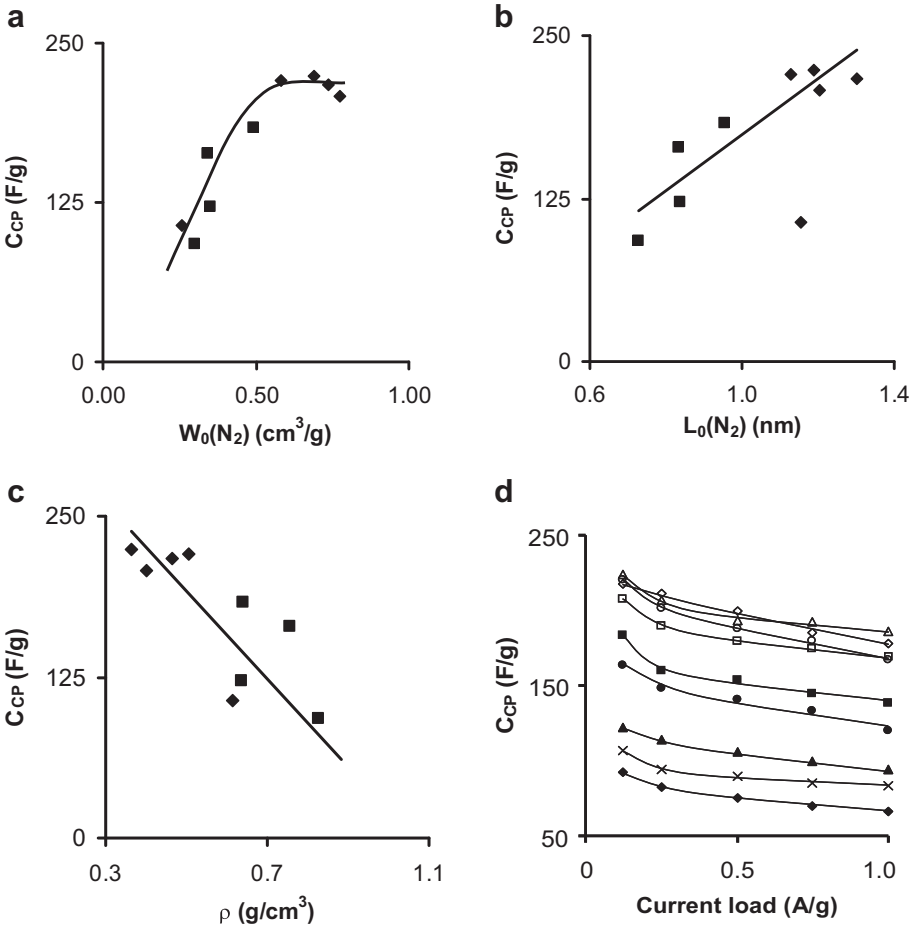

Fig. 7. Relationships between the gravimetric capacitance (C_{CP}) and total micropore volume (a), and mean micropore size (b) and particle density (c); CR series, ◆ and CP series, ■. (d) Variation of C_{CP} with current load in samples: CR (×), CR2 (◇), CR4 (□), CR4O (○), CR4N (△), CP2 (◆), CP4 (■), CP4O (●), and CP4N (▲).

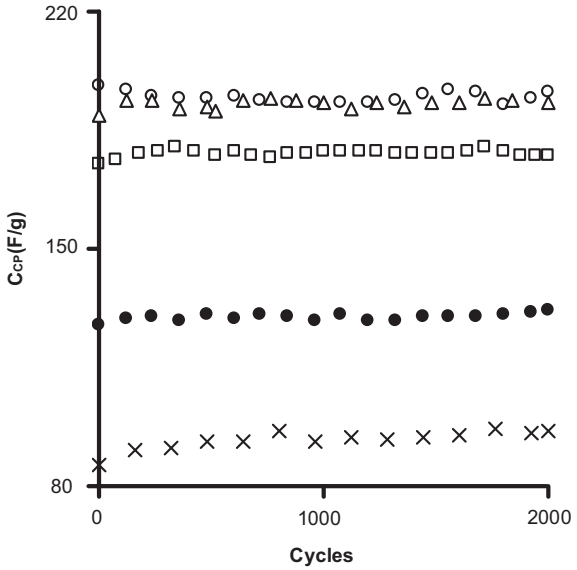

Fig. 8. Variation of the gravimetric capacitance (C_{CP}) with the number of charge–discharge cycles at 0.5 A g^{-1} in the potential window between 0 and 0.75 V. Samples CR (×), CR4 (□), CR4O (○), CR4N (△) and CP4O (●).

Fig. 7d depicts the variation of C_{CP} against the current load in the interval between 0.125 and 1 A g^{-1}, showing a decrease in its value with higher current load. The retention of capacitance at the highest current load (Table 5) is greater in samples from CR series (around 80%) than in samples from CP series (around 70%). This is because CR series samples have a higher volume of mesopores smaller than 4 nm in comparison to the CP series, favoring the transport of ions through the carbon porosity at a fast charge–discharge rate.

The long-term stability of electrodes is an important factor that limits the application of carbon materials as supercapacitors. Fig. 8 depicts the variation in gravimetric capacitance with higher number of charge–discharge cycles at 0.5 A g^{-1} and in a potential range between 0 and 0.75 V. The samples exhibit practically no capacitance fading after 2000 cycles. These results are similar to previous findings for carbon xerogels [45] and activated carbons [6,46,47].

4. Conclusions

Two series of carbon and activated carbon aerogels were obtained, one micro-mesoporous and the other basically microporous. A surface area as high as 1935 m^2 g^{-1} is obtained after KOH-activation of one of the carbon aerogels. Introduction of surface O and N functionalities on the activated carbon aerogels produces changes in porosity and surface area as detected by N_2 and CO_2 adsorption at −196 and 0 °C, respectively. The changes also affect the surface chemistry of the samples. Thus, an increase in the total or surface oxygen content of the samples produces a linear decrease in their hydrophobicity.

The gravimetric capacitance increases with total micropore volume, reaching the maximum value between 0.6 and 0.75 cm^3 g^{-1} and rising linearly with the mean size of the total microporosity within the microporosity range studied. The highest gravimetric capacitance at 0.125 A g^{-1}, around 220 F g^{-1}, is obtained with micro-mesoporous O- and N-doped activated carbon aerogels (CR4O and CR4N). The retention of capacitance at 1 A g^{-1} is around 80% in these samples *versus* 70% in the basically microporous samples. The gravimetric capacitance also linearly decreases with increasing particle density.

The highest volumetric capacitance, 123 F cm^{-3}, is obtained with the basically microporous O-doped activated carbon aerogel (CP4O), although it does not show the highest gravimetric capacitance (164 F g^{-1}). It is noteworthy that the volumetric capacitance of this sample is two-fold higher than is required for practical applications, supporting its suitability for utilization in small-volume systems.

Acknowledgments

This research was financed by the Junta de Andalucía. ZZB acknowledges a pre-doctoral fellowship from COLCIENCIAS, Colombia.

Appendix A. Supplementary data

Supplementary data related to this article can be found online at http://dx.doi.org/10.1016/j.jpowsour.2012.07.036.

References

[1] B.E. Conway, Electrochemical Supercapacitors. Scientific Fundamentals and Technological Applications, Kluwer Academic/Plenum, New York, 1999.
[2] K. Kinoshita, Carbon: Electrochemical and Physicochemical Properties, Wiley, New York, 1988.
[3] H. Shi, Electrochim. Acta 41 (1996) 1633–1639.
[4] E. Frackowiak, F. Beguin, Carbon 39 (2001) 937–950.
[5] A.G. Pandolfo, A.F. Hollenkamp, J. Power Sources 157 (2006) 11–27.
[6] E. Frackowiak, Phys. Chem. Chem. Phys. 9 (2007) 1774–1785.
[7] L.L. Zhang, X.S. Zhao, Chem. Soc. Rev. 38 (2009) 2520–2531.
[8] C.-T. Hsieh, H. Teng, Carbon 40 (2002) 667–674.
[9] G. Lota, B. Grzyb, H. Machnikowska, J. Machnikowski, E. Frackowiak, Chem. Phys. Lett. 404 (2005) 53–58.
[10] L. Zhao, L.Z. Fan, M.Q. Zhou, H. Guan, S. Qiao, M. Antonietti, M.-M. Titirici, Adv. Mater. 22 (2010) 5202–5206.
[11] H. Kim, M.E. Fortunato, H. Xu, J.H. Bang, K.S. Suslick, J. Phys. Chem. C 115 (2011) 20481–20486.
[12] A.M. ElKhatat, S.A. Al-Muhtaseb, Adv. Mater. 23 (2011) 2887–2903.
[13] C. Moreno-Castilla, in: P. Serp, J.L. Figueiredo (Eds.), Carbon Materials for Catalysis, J. Wiley & Sons, New York, 2009 (Chapter 10).
[14] R.W. Pekala, J.C. Farmer, C.T. Alviso, T.D. Tran, S.T. Mayer, J.M. Miller, B. Dunn, J. Non-Cryst. Solids 225 (1998) 74–80.
[15] S.W. Hwang, S.H. Hyun, J. Non-Cryst. Solids 347 (2004) 238–245.
[16] J. Li, X. Wang, Q. Huang, S. Gamboa, P.J. Sebastian, J. Power Sources 158 (2006) 784–788.
[17] C. Moreno-Castilla, F. Carrasco-Marín, M.V. López-Ramón, M.A. Álvarez-Merino, Carbon 39 (2001) 1415–1420.
[18] M.A. Lillo-Ródenas, D. Cazorla-Amorós, A. Linares-Solano, Carbon 41 (2003) 267–275.
[19] R. Ubago-Pérez, F. Carrasco-Marín, D. Fairén-Jiménez, C. Moreno-Castilla, Micropor. Mesopor. Mater. 92 (2006) 64–70.
[20] L. Zubizarreta, A. Arenillas, J.P. Pirard, J.J. Pis, N. Job, Micropor. Mesopor. Mater. 115 (2008) 480–490.
[21] B. Fang, L. Binder, J. Power Sources 163 (2006) 616–622.
[22] C. Moreno-Castilla, F. Carrasco-Marín, A. Mueden, Carbon 35 (1997) 1619–1626.
[23] M. Seredych, D. Hulicova-Jurcakova, Q.L. Gao, T.J. Bandosz, Carbon 46 (2008) 1475–1488.
[24] F. Stoeckli, in: J.W. Patrick (Ed.), Porosity in Carbons: Characterization and Applications, Edward Arnold, London, 1995. p. 66.
[25] K.S.W. Sing, D.H. Everett, R.A.W. Haul, L. Moscou, R.A. Pierotti, J. Rouquerol, T. Siemieniewska, Pure Appl. Chem. 57 (1985) 603–619.
[26] C. Moreno-Castilla, M.B. Dawidziuk, F. Carrasco-Marín, Z. Zapata-Benabithe, Carbon 49 (2011) 3808–3819.
[27] F. Rodríguez-Reinoso, A. Linares-Solano, in: P.A. Thrower (Ed.), Chemistry and Physics of Carbon, vol. 21, Marcel Dekker, New York, 1989, p. 1.
[28] D. Cazorla-Amorós, J. Alcañiz-Monge, M.A. De la Casa-Lillo, A. Linares-Solano, Langmuir 14 (1998) 4589–4596.
[29] U. Zielke, K.J. Huttinger, W.P. Hoffman, Carbon 34 (1996) 983–998.
[30] J. Surygala, R. Wandas, E. Sliwka, Fuel 72 (1993) 409–411.
[31] S. Haydar, C. Moreno-Castilla, M.A. Ferro-García, F. Carrasco-Marín, J. Rivera-Utrilla, A. Perrard, J.P. Joly, Carbon 38 (2000) 1297–1308.
[32] P.J. Hall, J.M. Calo, Energy Fuels 3 (1989) 370–376.
[33] J.M. Calo, P.J. Hall, in: J. Lahaye, P. Ehrburger (Eds.), Fundamental Issues in the Control of Carbon Gasification and Reactivity, Kluwer Academic Publications, Dordrecht, The Netherlands, 1991. p. 329.

[34] E. Desimoni, G.I. Casella, A.M. Salvi, Carbon 30 (1992) 521–526.
[35] J.R. Pels, F. Kapteijn, J.A. Moulijn, Q. Zhu, K.M. Thomas, Carbon 33 (1995) 1641–1653.
[36] F. Kapteijn, J.A. Moulijn, S. Matzner, H.P. Boehm, Carbon 37 (1999) 1143–1150.
[37] M. Pérez-Cadenas, C. Moreno-Castilla, F. Carrasco-Marín, A.F. Pérez-Cadenas, Langmuir 25 (2009) 466–470.
[38] M. Koh, T. Nakajima, Carbon 38 (2000) 1947–1954.
[39] D. Hulicova, J. Yamashita, Y. Soneda, H. Hatori, M. Kodama, Chem. Mater. 17 (2005) 1241–1247.
[40] Z.H. Zhu, H. Hatori, S.B. Wang, G.Q. Lu, J. Phys. Chem. B 109 (2005) 16744–16749.
[41] G. Salitra, A. Soffer, L. Eliad, Y. Cohen, D. Aurbach, J. Electrochem. Soc. 147 (2000) 2486–2493.
[42] O. Barbieri, M. Hahn, A. Herzog, R. Kötz, Carbon 43 (2005) 1303–1310.
[43] C. Moreno-Castilla, M.B. Dawidziuk, F. Carrasco-Marín, E. Morallón, Carbon (2012). http://dx.doi.org/10.1016/j.carbon.2011.12.047.
[44] W. Li, G. Reichenauer, J. Fricke, Carbon 40 (2002) 2955–2959.
[45] E.G. Calvo, C.O. Ania, L. Zubizarreta, J.A. Menéndez, A. Arenillas, Energy Fuels 24 (2010) 3334–3339.
[46] C. Portet, P.L. Taberna, P. Simon, E. Flahaut, C. Laberty-Robert, Electrochim. Acta 50 (2005) 4174–4181.
[47] V. Khomenko, E. Raymundo-Piñero, F. Béguin, J. Power Sources 177 (2008) 643–651.